Journal of Nuclear Medicine, published on December 5, 2019 as doi:10.2967/jnumed.119.233411

Radiation Dosimetry in ^{177}Lu-PSMA-617 Therapy Using a Single Post-treatment SPECT/CT: A Novel Methodology to Generate Time- and Tissue-specific Dose Factors

Price A Jackson

[1]Department of Cancer Imaging, Peter MacCallum Cancer Centre

[2]The Sir Peter MacCallum Department of Oncology, University of Melbourne

Corresponding Author:

305 Grattan St, Melbourne VIC, 3000 Australia

Price.Jackson@petermac.org

Tel: +61 3 8559 8729

Fax: +61 3 8559 6929

Michael S Hofman

[1]Department of Cancer Imaging, Peter MacCallum Cancer Centre

[2]The Sir Peter MacCallum Department of Oncology, University of Melbourne

Rodney J Hicks

[1]Department of Cancer Imaging, Peter MacCallum Cancer Centre

[2]The Sir Peter MacCallum Department of Oncology, University of Melbourne

Mark Scalzo

[1]Department of Cancer Imaging, Peter MacCallum Cancer Centre

John Violet

[3]Department of Radiation Oncology, Peter MacCallum Cancer Centre

Word Count: 4,977

Running Title: Single Time Point Lu-PSMA Dosimetry

Key Words: Lu-PSMA-617, Radiation Dosimetry, Radiobiology, Image Processing

Disclosure:

PJ is supported by the Victorian Cancer Agency. MSH is supported by a Clinical Fellowship Award from the Peter MacCallum Foundation and receives research support from Endocyte (a Novartis company). RJH is recipient of a National Health and Medical Research Council Practitioner Fellowship (APP1108050). ^{177}Lu was supplied by the Australian Nuclear Science and Technology Organisation (ANSTO) and PSMA-617 by Endocyte (a Novartis company) and Advanced Biochemical Compounds (ABX, Radeberg, Germany). RH holds stock in Telix Pharmaceuticals on behalf of the Peter MacCallum Cancer Centre with all dividends donated to his department. No other potential conflicts of interest relevant to this article exist.

Abstract:

Calculation of radiation dosimetry in targeted nuclear medicine therapies is traditionally resource-intensive requiring multiple post-therapy SPECT acquisitions. An alternative approach is to take advantage of existing pharmacokinetic data from these smaller cohorts to enable dose computation from a single post-treatment scan in a manner that may be applied to a much broader patient population. **Methods:** In this work, a technical description for simplified dose estimation is presented and applied to assessment of ^{177}Lu-PSMA-617 therapy (Prostate-Specific Membrane Antigen) for metastatic prostate cancer. By normalizing existing time-activity curves to a single measurement time, it is possible to calculate a mean and range of time-integrated activity values which relate to radiation absorbed dose. To assist with accurate pharmacokinetic modelling of the training cohort, a method for contour-guided image registration was developed. **Results:** Tissue-specific dose conversion factors for common post-treatment imaging times are reported along with a characterization of added uncertainty in comparison to a traditional serial imaging protocol. Single time point dose factors for tumor were determined to be 11.0, 12.1, 13.6, and 15.2 Gy per MBq/mL at image times of 24, 48, 72, and 96 hours, respectively. For normal tissues, parotid gland factors were 6.7, 9.4, 13.3, and 19.3 Gy per MBq/mL and kidneys were 7.1, 10.3, 15.0, and 22.0 Gy per MBq/mL at those times. Tumor dose estimates were most accurate using delayed scanning at times beyond 72 hours. Dose to healthy tissues is best characterized by scanning patients in the first two days of treatment owing to the larger degree of tracer clearance in this early phase. **Conclusion:** The work demonstrates a means for efficient dose estimation in ^{177}Lu-PSMA-617 therapy. By providing methods to simplify and potentially automate radiation dosimetry we hope to accelerate the understanding of radiobiology and development of dose-response models in this unique therapeutic context.

Text:

Introduction

The accurate determination of absorbed radiation dose in normal tissues and tumor is key to the optimal development of all forms of radiotherapy. In external beam radiotherapy, where the dose in tissues and tumor can be reliably controlled, dose response relationships have been well established (*1*) and shown to determine the likelihood of response and toxicity. Radiation dosimetry is also key to the optimal development of directed radionuclide therapy but carries different logistical challenges which limit its application in routine practice. As a result, many response relationships in targeted therapies are not clearly established.

A novel form of therapy for prostate cancer uses radiolabeled small molecules targeting prostate specific membrane antigen (PSMA). This is overexpressed in most prostate cancers (*2,3*) and PSMA expression is limited in non-prostatic tissues (*4,5*) making it a highly attractive target for prostate cancer. Nevertheless, clinically, high uptake is observed in the salivary glands, duodenum and kidneys. Of these, radiation sialadenitis with failure of adequate saliva production poses a significant issue with respect to quality of life of patients receiving this therapy (*6*).

Treatment with ^{177}Lu-PSMA-617, labelled with the β-emitting radionuclide Lutetium-177 demonstrates high activity and low acute toxicity in men with advanced cancer in both retrospective (*7-12*) and prospective clinical trials (*13*). Detailed voxel-based radiation dosimetry was performed in the latter cohort with three time point quantitative SPECT/CT imaging at 4, 24 and 96 hours (*14*). This showed that 'whole body' tumor absorbed dose was a predictor of biochemical response and that absorbed dose in normal tissues showed wide variation between patients. High uptake and retention of radiation occurred within tumor, whilst normal tissues receiving the highest radiation dose included salivary and lacrimal glands and the kidneys, findings concordant with other reported dosimetry data (*7,14-20*).

To date, most radiation dosimetry using radiolabeled PSMA has incorporated the Medical Internal Radiation Dosimetry (MIRD) schema (*21-23*). This involves computation of time-activity curves which are integrated to quantify disintegrations and converted into absorbed dose using a factor that approximates radiation transport for a given isotope and physical material (*24,25*). With beta-emitting isotopes, the absorbed dose is closely proportional to the integral number of disintegrations in a region of uptake (*26,27*). Typical application of MIRDrequires sequential scans and manual drawing of multiple regions of interest, a process that can be overly time- and resource-intensive. Techniques to simplify dose estimation from a single measurement have been described by Madsen *et al. (28)* and Hänscheid *et al.* (*29*). These works offer similar approaches to infer time integrated activity based on a single measurement by using a generic effective half-time or mixture of exponential/bi-exponential kinetic parameters.

The aim of this work is to expand on previous methods for single-time point dosimetry with application to tumor and at-risk organs followed administration of ^{177}Lu-PSMA-617. The developed methodology determines local time-integrated activity for any post-treatment image time and preserves the kinetic parameters of all training cases to permit assessment according to population mean with an associated error analysis. In its development, the work also illustrates an efficient method to measure uptake on serial imaging by focusing on each region individually to improve spatial accuracy.

Materials and Methods

Lu-PSMA Therapy and Image Acquisition:

Thirty patients were enrolled and underwent therapy with ^{177}Lu-PSMA-617 for metastatic castration-resistant prostate cancer (*30*). The trial was registered with the Australian New Zealand Clinical Trials Registry (ANZCTR12615000912583) and reviewed by the local institutional review board. All patients gave written informed consent before entry. Following the first cycle of therapy, patients were imaged

with serial post-treatment quantitative SPECT imaging at 4, 24, and 96 hours to characterize radiotracer pharmacokinetics in tumor and normal tissues-of-interest. Twenty-nine patients were available for analysis with complete multi-phase image series. Each imaging system (Siemens Symbia T6 or Intevo 16) was calibrated for quantitative imaging with Lutetium-177 according to a previously described method (*31*) yielding volumetric images in pseudo-PET format: voxel intensity in units of Bq/mL.

Image Alignment and Biodistribution Analysis:

Pharmacokinetics for each organ was characterized with a tri-exponential model to account for an initial phase of uptake as well as rapid and long-term clearance phases (*27*). The model is given in equation 1, with the amplitude of the initial uptake phase (A_1) equivalent to the negative sum of the two clearance phases ($A_2 + A_3$) yielding curves which pass through zero at t=0. The selection of post-treatment imaging time points and model considered both the physical half-life of ^{177}Lu (6.7 days) and the variety of target and at-risk tissues relevant to PSMA-directed therapy.

Eq. 1 $$Activity = -A_1 * e^{-k_1 * t} + A_2 * e^{-k_2 * t} + A_3 * e^{-k_3 * t}$$

Based on previous evaluation (*32*), regions that exhibited reliable image-based measurements for characterizing tissue kinetics included: tumor, parotid glands, submandibular glands, liver, kidney and spleen. Lacrimal glands were outside the field-of-view at some time points and subject to significant partial volume effects rendering them unreliable for developing a population model. Red bone marrow was omitted from the analysis due to the majority of the patient cohort displaying osseous disease infiltration that did not permit consistent measurement of reproducible marrow regions.

[Figure 1]

To evaluate serial measurements, 3D volumes-of-interest were defined on the 4-hour image volume. Subsequent images were aligned for each contour independently. The two-stage process first utilized a

rigid CT-to-CT registration of the full image volume to achieve a gross initial alignment (*33*). Each volume-of-interest was then selected as a masked sub-region and a fine-level registration was performed using only the voxels in the structure plus an expanded range of 5-8 centimeters to provide boundary information. Contours with focal uptake on functional imaging such as tumor and parotid glands were guided by intensity on SPECT while regions with clear structural margins and relatively uniform uptake such as kidney and liver were fused based on CT Hounsfield values. Following alignment, each contour was reviewed for accuracy at each of the three time points by colored overlay maximum-intensity projection image as shown in Figure 1. Computer code to automate sequential contour-guided image registration and generation of MIP images have been made available online for general use (*34*).

Single Time Point Pharmacokinetics Normalization:

The curve fitting parameters from each subject or organ pair with visually acceptable alignment were tabulated to generate a population pharmacokinetic model for each tissue type. Those with unsatisfactory agreement were excluded from further analysis. In total, 226 tumor regions were included while 45, 43, 57, 27, and 28 regions were evaluated for parotid gland, submandibular gland, kidney, liver, and spleen, respectively. In order to normalize for a single post-therapy image measurement, each time activity curve in the population model was multiplied by a single scaling factor, which modified the relative height, or amplitude, of the curve while preserving the kinetic parameters, $k_{1\text{-}3}$ and the relative contribution of each uptake and clearance phase. Using this method, the curves may be normalized to any post-injection time point including intermediate values that lie between the times used for initial modelling.

Eq. 2-1 $$Act(t) = S_p(t) * \left(-A_{p,1} * e^{-k_{p,1}*t} + A_{p,2} * e^{-k_{p,2}*t} + A_{p,3} * e^{-k_{p,3}*t}\right)$$

$$\text{Eq. 2-2 } S_p(t) = \frac{Act(t)}{\left(-A_{p,1} * e^{-k_{p,1} * t} + A_{p,2} * e^{-k_{p,2} * t} + A_{p,3} * e^{-k_{p,3} * t}\right)}$$

$$\text{Eq. 2-3 } \tilde{A}_p = \int_0^{\infty} Act(t) * dt$$

$$\text{Eq. 2-4 } \tilde{A}_p = S_p(t) * \left(\frac{-A_{p,1}}{k_{p,1}} + \frac{A_{p,2}}{k_{p,2}} + \frac{A_{p,3}}{k_{p,3}}\right)$$

$$\text{Eq. 2-5 } \overline{\tilde{A}_p} = \frac{\sum_{p=1}^{n} S_p(t) * \left(\frac{-A_{p,1}}{k_{p,1}} + \frac{A_{p,2}}{k_{p,2}} + \frac{A_{p,3}}{k_{p,3}}\right)}{n}$$

Where $A_{p,1\text{-}3}$ and $k_{p,1\text{-}3}$ are the best-fit parameters for an organ-of-interest for patient p. The scaling factor $S_p(t)$ modifies the height of the curve in order to match the measured activity, $Act(t)$, at time t for a single measurement time as shown in Figure 2. For each patient reference curve, a unique scaling factor can be calculated according to Equation 2-2. The integral time-integrated activity, $\tilde{A}$, is then taken for all of the normalized curves as shown in Equation 2-4. A detailed derivation is provided in the supplementary material. As a population model, the mean and average error for each patient and time point relative to the original three time point measured value is reported. To avoid subtle bias, this model is recalculated omitting each patient's own pharmacokinetic data and given as the quantity mean absolute deviation. For images reconstructed and calibrated in units of activity concentration (Bq/mL), multiplying by the time-integrated activity factor (hours) yields a measure of disintegrations per unit volume (Bq*h/mL). Absorbed dose (Gy) may be calculated by multiplying by a radiation transport S-factor to a representative tissue medium. For tissue with a nominal density of 1.0 g/ml with ^{177}Lu, the factor is approximated at 8.67E-5 Gy/(kBq*h/mL) by OLINDA sphere model which exhibits little dependence on physical size (see Supplemental Figure 1) (*23*).

[Figure 2]

Results:

The described image measurement method provided reliable contour matching across serial time points for the majority of images in both tumor and healthy organs. For each patient between 8-12 individual tumor contours were delineated. Of the initial 260 regions, 226 (87%) displayed visually clear 3D alignment across all three post-treatment imaging time points and were included in the pharmacokinetics analysis (*34*). The results for all included organs are reported in Table 1.

[Figure 3]

[Table 1]

For tumor and normal organs, measurements of activity concentration on a single image were correlated with time-integrated activity as estimated by serial imaging. Organ- and time-specific conversion factors are presented in Table 2 to multiply activity concentration into an estimate of decays per unit volume (Bq*h/mL). With the addition of a radiation transport S-factor, it is possible to directly estimate radiation absorbed dose (Gy) from quantitative SPECT images at a given time post-administration. Time-integrated activity conversion factors for tumor with images acquired at 24, 48, and 96 h post-injection equate to 127, 140, and 176 h, respectively. For parotid glands, factors at those time points are 77, 108, 222 hours; indicative of the relative difference in pharmacological clearance between tissue types.

The selection of imaging time is related to the precision of dose estimate and varies depending on region. In tumor, the predicted single time point dose is more reliable with delayed acquisitions at two days or beyond. At 48 hours, the mean absolute difference between the simplified single measurement model and serial imaging is 14.3% of the predicted time-integrated activity value. At 72 and 96 hours the error as a percentage decreases to 9.3 and 5.1, respectively. This is indicative of the prolonged retention of ^{177}Lu-PSMA in tumor where the proportion of disintegrations for the 6.7 day half-life isotope is largely influenced by the slow wash-out phase. The range of normalized time-activity curves for tumor are

illustrated in Figure 3 showing the variety of temporal shapes across the population as well as the representative mean and integral shaded area as a blend of all modelled curves.

[Table 2]

By contrast, healthy tissues with primary uptake followed by relatively efficient washout were poorly characterized for dosimetry on delayed phase imaging as retention at 96 hours not representative of early activity concentration values. The minimum uncertainty using the single time point model for parotid glands occurs at approximately 48 hours post-administration (3.9% of mean) increasing to over 20% beyond 96 hours. Figure 4 illustrates dose factors for each tissue along with the relative uncertainty in applying a single-time point model compared to serial imaging as a function of imaging time. A tabulated list of common imaging time points is given in Table 2 and values for of all intermediate time values are reported in Supplemental Tables 1-3. To illustrate, for a lesion with measuring a mean activity concentration of 1,500 kBq/mL at 96 hours post-injection, the time-integrated activity factor is determined to be 176h ± 5% and using nominal soft tissue S-factor of 8.7E-5 Gy per (kBq*h/mL), radiation dose is estimated at 22.8 ± 1.2 Gy.

[Figure 4]

Discussion:

Using data from patients treated with ^{177}Lu-PSMA-617 on a prospective trial with serial imaging (*30*), we describe two novel methodologies for the application of radiation dosimetry. The first provides an automated means to perform contour-guided alignment of functional images using DICOM-RT structure sets. When linked to a pharmacokinetic interpolation algorithm provides a reliable means of characterizing tracer clearance. Even for small structures such as parotid and submandibular glands

where activity measurements are unreliable with displacements of several millimeters, the automated workflow achieved satisfactory co-registration across all three time points at a rate of 75%.

The second reports the ability of a single time point measurement to assess dosimetry in normal tissues and tumor. This takes advantage of previously recorded pharmacokinetic data from a representative cohort in a manner that is similar to the works of Madsen and Hänscheid (*28,29,35*). While previous works determine generic pharmacokinetic parameters for each tissue, in this method all input curves are preserved and normalized independently, facilitating analysis of mean and associated uncertainties at any time point. The model may be updated with data derived from images acquired at different post-administration timelines and may, in principle, incorporate data from any continuous pharmacokinetic function. Average deviation from single- and multi-time point measurements indicates that the most reliable range of image times to predict radiation dose varies depending on the organ or tissue of interest. The finding is in accordance with a previous work identifying normal tissue clearance has largely completed within the first 48 hours post-administration (*36*) while tumor retention is more closely reflected by the physical half-life of lutetium-177.

If coupled to image segmentation algorithms, such as those emerging through developments in convolutional neural network image recognition, there is a straightforward roadmap to fully automate dose reporting based on routine imaging follow-up (*37-39*). The long-term aim of these investigations is to provide individualized therapy based upon a patients known physiology using a validated rationale to administer a personalized maximum tolerated dose and so optimize the therapeutic ratio of treatment (*40*). We have demonstrated in previous work that biochemical response is related to “whole body” tumor dose but we have not clearly reported a relationship between dose and acute normal tissue toxicity; though this may be due to the lack of acute toxicity that has been observed in the clinical application of ^{177}Lu-PSMA-617 to date (*13*). Additionally, the pharmacokinetic models may be decoupled

from the physical half-life lutetium-177 and applied to other therapeutic tracers by decay-correcting and using an appropriate radiation transport dose factor. In this manner, the same methodology may be applied to single time point dose factors generate factors for, for example, ^{90}Y-PSMA-617 therapy under the assumption that the tracer has comparable pharmacological biodistribution and clearance kinetics (*41*).

In the long term it is hoped that this methodology can be expanded with additional multi-time point data either locally or from other centers to improve the overall accuracy of the model and potentially identify predictors of patients as either slow- or fast-clearing which may become apparent across a broader population of sampling of data. It would also be worthwhile to investigate whether organ time-activity curves are interdependent within a patient. That is, in this evaluation it is assumed that organ clearance is not affected by the kinetic models in other tissues.

Conclusion:

This work presents a means of estimating radiation dosimetry for ^{177}Lu-PSMA therapy based on readily available post-treatment imaging for a single time point. A novel method of predicting time-integrated activity using a population of normalized pharmacokinetic curves is illustrated; one that may incorporate data from a variety of imaging timelines and interpolate dose coefficients for any intermediate times. This aims to improve dose-response modelling by enabling simplified radiation dose estimates from a broad cohort of patients receiving molecular radiotherapy as opposed to only those on trials involving comprehensive follow-up imaging.

Disclosure:

PJ is supported by a Fellowship from the Victorian Cancer Agency. MSH is supported by a Clinical Fellowship Award from the Peter MacCallum Foundation and receives research support from Endocyte

(a Novartis company). RJH is recipient of a National Health and Medical Research Council Practitioner Fellowship (APP1108050). 177Lu (no carrier added) was supplied by the Australian Nuclear Science and Technology Organisation (ANSTO) and PSMA-617 by Endocyte (a Novartis company) and Advanced Biochemical Compounds (ABX, Radeberg, Germany). RH holds stock in Telix Pharmaceuticals on behalf of the Peter MacCallum Cancer Centre with all dividends donated to his department. No other potential conflicts of interest relevant to this article exist.

Key Points:

Question: Is it possible to obtain reliable radiation dose estimates to tumor and at-risk organs based on one follow-up quantitative SPECT/CT in treatment of prostate cancer with 177Lu-PSMA-617?

Pertinent Findings:

Using a pilot cohort of 29 patients with serial post-treatment imaging, a novel method of incorporating existing pharmacokinetic models was developed to predict dosimetry from a single post-therapy image. The method presents conversion factors to estimate absorbed dose from measured activity concentration along with a characterization of added uncertainty by using the simplified model. Findings show the ideal imaging time yield accurate dose estimates across tissue types is in the window of 2-3 days post-administration of 177Lu-PSMA-617.

Implications for Patient Care:

The technique permits radiation dose calculation in routine follow-up of PSMA therapy as would be standard at many clinical centers. Absorbed Dose may be considered as a more robust metric to inform ongoing management and optimize prescription of subsequent treatment cycles compared to traditional measures of uptake such as SUV. Additionally, by collecting dosimetry from a broader cohort of patients this technique should accelerate the understanding of radiobiology and potential for treatment personalization in targeted radionuclide therapies.

References

1. Marks LB, Yorke ED, Jackson A, et al. Use of normal tissue complication probability models in the clinic. *Int J Radiat Oncol Biol Phys.* 2010;76:S10-19.

2. Smith-Jones PM, Vallabhajosula S, Navarro V, Bastidas D, Goldsmith SJ, Bander NH. Radiolabeled monoclonal antibodies specific to the extracellular domain of prostate-specific membrane antigen: preclinical studies in nude mice bearing LNCaP human prostate tumor. *J Nucl Med.* 2003;44:610-617.

3. Ghosh A, Heston WD. Tumor target prostate specific membrane antigen (PSMA) and its regulation in prostate cancer. *J Cell Biochem.* 2004;91:528-539.

4. Troyer JK, Beckett ML, Wright GL, Jr. Detection and characterization of the prostate-specific membrane antigen (PSMA) in tissue extracts and body fluids. *Int J Cancer.* 1995;62:552-558.

5. Sokoloff RL, Norton KC, Gasior CL, Marker KM, Grauer LS. A dual-monoclonal sandwich assay for prostate-specific membrane antigen: levels in tissues, seminal fluid and urine. *Prostate.* 2000;43:150-157.

6. Taïeb D, Foletti J-M, Bardiès M, Rocchi P, Hicks RJ, Haberkorn U. PSMA-targeted radionuclide therapy and salivary gland toxicity: why does it matter? *Journal of Nuclear Medicine.* 2018;59:747-748.

7. Zechmann CM, Afshar-Oromieh A, Armor T, et al. Radiation dosimetry and first therapy results with a (124)I/ (131)I-labeled small molecule (MIP-1095) targeting PSMA for prostate cancer therapy. *Eur J Nucl Med Mol Imaging.* 2014;41:1280-1292.

8. Ahmadzadehfar H, Rahbar K, Kurpig S, et al. Early side effects and first results of radioligand therapy with (177)Lu-DKFZ-617 PSMA of castrate-resistant metastatic prostate cancer: a two-centre study. *EJNMMI Res.* 2015;5:114.

9. Rahbar K, Ahmadzadehfar H, Kratochwil C, et al. German multicenter study investigating 177Lu-PSMA-617 radioligand therapy in advanced prostate cancer patients. *J Nucl Med.* 2017;58:85-90.

10. Kratochwil C, Giesel FL, Stefanova M, et al. PSMA-targeted radionuclide therapy of metastatic castration-resistant prostate cancer with Lu-177 labeled PSMA-617. *J Nucl Med.* 2016.

11. Heck MM, Retz M, D'Alessandria C, et al. Systemic Radioligand Therapy with (177)Lu Labeled Prostate Specific Membrane Antigen Ligand for Imaging and Therapy in Patients with Metastatic Castration Resistant Prostate Cancer. *J Urol.* 2016;196:382-391.

12. Yadav MP, Ballal S, Tripathi M, et al. 177Lu-DKFZ-PSMA-617 therapy in metastatic castration resistant prostate cancer: safety, efficacy, and quality of life assessment. *Eur J Nucl Med Mol Imaging.* 2016.

13. Hofman MS, Violet J, Hicks RJ, et al. [(177)Lu]-PSMA-617 radionuclide treatment in patients with metastatic castration-resistant prostate cancer (LuPSMA trial): a single-centre, single-arm, phase 2 study. *Lancet Oncol.* 2018;19:825-833.

14. Violet J, Jackson P, Ferdinandus J, et al. Dosimetry of (177)Lu-PSMA-617 in Metastatic Castration-Resistant Prostate Cancer: Correlations Between Pretherapeutic Imaging and Whole-Body Tumor Dosimetry with Treatment Outcomes. *J Nucl Med.* 2019;60:517-523.

15. Hohberg M, Eschner W, Schmidt M, et al. Lacrimal Glands May Represent Organs at Risk for Radionuclide Therapy of Prostate Cancer with [Lu]DKFZ-PSMA-617. *Mol Imaging Biol.* 2016.

16. Delker A, Fendler WP, Kratochwil C, et al. Dosimetry for (177)Lu-DKFZ-PSMA-617: a new radiopharmaceutical for the treatment of metastatic prostate cancer. *Eur J Nucl Med Mol Imaging.* 2016;43:42-51.

17. Kabasakal L, AbuQbeitah M, Aygun A, et al. Pre-therapeutic dosimetry of normal organs and tissues of (177)Lu-PSMA-617 prostate-specific membrane antigen (PSMA) inhibitor in patients with castration-resistant prostate cancer. *Eur J Nucl Med Mol Imaging.* 2015;42:1976-1983.

18. Okamoto S, Thieme A, Allmann J, et al. Radiation dosimetry for 177Lu-PSMA-I&T in metastatic castration-resistant prostate cancer: Absorbed dose in normal organs and tumor lesions. *J Nucl Med.* 2016.

19. Yadav MP, Ballal S, Tripathi M, et al. Post-therapeutic dosimetry of 177Lu-DKFZ-PSMA-617 in the treatment of patients with metastatic castration-resistant prostate cancer. *Nucl Med Commun.* 2017;38:91-98.

20. Fendler WP, Kratochwil C, Ahmadzadehfar H, et al. [177Lu-PSMA-617 therapy, dosimetry and follow-up in patients with metastatic castration-resistant prostate cancer]. *Nuklearmedizin.* 2016;55:123-128.

21. Hindorf C, Glatting G, Chiesa C, Linden O, Flux G. EANM Dosimetry Committee guidelines for bone marrow and whole-body dosimetry. *Eur J Nucl Med Mol Imaging.* 2010;37:1238-1250.

22. Siegel JA, Thomas SR, Stubbs JB, et al. MIRD pamphlet no. 16: Techniques for quantitative radiopharmaceutical biodistribution data acquisition and analysis for use in human radiation dose estimates. *J Nucl Med.* 1999;40:37S-61S.

23. Stabin MG, Sparks RB, Crowe E. OLINDA/EXM: the second-generation personal computer software for internal dose assessment in nuclear medicine. *Journal of nuclear medicine.* 2005;46:1023-1027.

24. Bolch WE, Bouchet LG, Robertson JS, et al. MIRD pamphlet no. 17: the dosimetry of nonuniform activity distributions—radionuclide S values at the voxel level. *Journal of Nuclear Medicine.* 1999;40:11S-36S.

25. Watson EE, Stabin MG, Siegel JA. MIRD formulation. *Medical physics.* 1993;20:511-514.

26. Bolch WE, Eckerman KF, Sgouros G, Thomas SR. MIRD pamphlet no. 21: a generalized schema for radiopharmaceutical dosimetry—standardization of nomenclature. *Journal of Nuclear Medicine.* 2009;50:477-484.

27. Jackson PA, Beauregard JM, Hofman MS, Kron T, Hogg A, Hicks RJ. An automated voxelized dosimetry tool for radionuclide therapy based on serial quantitative SPECT/CT imaging. *Medical physics.* 2013;40.

28. Madsen MT, Menda Y, O'Dorisio TM, O'Dorisio MS. Single time point dose estimate for exponential clearance. *Medical physics.* 2018;45:2318-2324.

29. Hänscheid H, Lapa C, Buck AK, Lassmann M, Werner RA. Dose mapping after endoradiotherapy with 177Lu-DOTATATE/DOTATOC by a single measurement after 4 days. *Journal of Nuclear Medicine.* 2018;59:75-81.

30. Hofman MS, Violet J, Hicks RJ, et al. [177Lu]-PSMA-617 radionuclide treatment in patients with metastatic castration-resistant prostate cancer (LuPSMA trial): a single-centre, single-arm, phase 2 study. *The Lancet Oncology.* 2018;19:825-833.

31. Beauregard J-M, Hofman MS, Pereira JM, Eu P, Hicks RJ. Quantitative 177Lu SPECT (QSPECT) imaging using a commercially available SPECT/CT system. *Cancer Imaging.* 2011;11:56.

32. Violet JA, Jackson P, Ferdinandus J, et al. Dosimetry of 177Lu-PSMA-617 in metastatic castration-resistant prostate cancer: correlations between pretherapeutic imaging and whole-body tumor dosimetry with treatment outcomes. *Journal of Nuclear Medicine.* 2019;60:517-523.

33. Klein S, Staring M, Murphy K, Viergever MA, Pluim JP. Elastix: a toolbox for intensity-based medical image registration. *IEEE transactions on medical imaging.* 2010;29:196-205.

34. Jackson PA. Contour-guided Registration. https://github.com/jacksonmedphysics/contour-guided-registration.

35. Hänscheid H, Lapa C, Buck AK, Lassmann M, Werner RA. Absorbed dose estimates from a single measurement one to three days after the administration of 177Lu-DOTATATE/-TOC. *Nuklearmedizin.* 2017;56:219-224.

36. Kratochwil C, Giesel FL, Stefanova M, et al. PSMA-targeted radionuclide therapy of metastatic castration-resistant prostate cancer with 177Lu-labeled PSMA-617. *Journal of Nuclear Medicine.* 2016;57:1170-1176.

37. Belal SL, Sadik M, Kaboteh R, et al. Deep Learning for Segmentation of 49 Selected Bones in CT Scans: First Step in Automated PET/CT-based 3D Quantification of Skeletal Metastases. *European Journal of Radiology.* 2019.

38. Jackson P, Hardcastle N, Dawe N, Kron T, Hofman MS, Hicks RJ. Deep learning renal segmentation for Fully automated radiation Dose estimation in Unsealed source Therapy. *Frontiers in oncology.* 2018;8.

39. Sjostrand K, Anand A, Richter J, et al. Automated detection and quantification of prostatic PSMA uptake in SPECT/CT using a deep learning algorithm for segmentation of pelvic anatomy. *Journal of Nuclear Medicine.* 2018;59:30-30.

40. Kabasakal L, Türkay Toklu NY, Demirci E, et al. Lu-177-PSMA-617 prostate-specific membrane antigen inhibitor therapy in patients with castration-resistant prostate cancer: stability, bio-distribution and dosimetry. *Molecular imaging and radionuclide therapy.* 2017;26:62.

41. Rathke H, Flechsig P, Mier W, et al. Dosimetry estimate and initial clinical experience with 90Y-PSMA-617. *Journal of Nuclear Medicine.* 2019;60:806-811.

Tables:

Organ	Patients	Total Regions in Analysis	Percentage of Available Contours
Tumor	29	226	86.9%
Parotid Gland	24	45	77.6%
Submandibular Gland	23	43	74.1%
Kidney	29	57	98.3%
Liver	27	27	93.1%
Spleen	28	28	96.6%

Table 1 - Number of patients and contours included for each tissue type in the population pharmacokinetic model. From the initial cohort, only regions with satisfactory 3D spatial alignment at all imaging time points and normal tissue regions free from tumor infiltration were considered reliable for analysis.

Image Time (hours)	Tumour	Parotid Gland	Submandibular Gland	Kidney	Liver	Spleen	Lacrimal Gland
12	129 ± 22%	65 ± 13%	66 ± 14%	62 ± 12%	76 ± 24%	80 ± 25%	85 ± 31%
18	126 ± 21%	71 ± 11%	71 ± 13%	74 ± 12%	91 ± 22%	100 ± 24%	87 ± 28%
24	127 ± 19%	77 ± 10%	77 ± 12%	82 ± 11%	99 ± 19%	110 ± 21%	92 ± 25%
36	133 ± 17%	91 ± 7%	91 ± 9%	99 ± 9%	115 ± 15%	127 ± 16%	103 ± 19%
48	140 ± 14%	108 ± 4%	107 ± 6%	119 ± 8%	131 ± 11%	145 ± 12%	117 ± 12%
60	148 ± 12%	129 ± 5%	127 ± 5%	144 ± 8%	151 ± 9%	167 ± 10%	134 ± 8%
72	156 ± 9%	154 ± 8%	151 ± 6%	173 ± 10%	175 ± 8%	193 ± 11%	154 ± 9%
96	176 ± 5%	222 ± 17%	217 ± 14%	254 ± 16%	235 ± 12%	262 ± 19%	211 ± 22%
120	198 ± 4%	328 ± 28%	314 ± 23%	375 ± 22%	321 ± 20%	361 ± 28%	300 ± 39%

Table 2 – Time-integrated activity factor (h) to convert single measurement (Bq/mL) into estimated time-integrated activity concentration (Bq*h/mL, disintegrations per unit volume). For normalized image time and tissue-of-interest the mean error of residence time as percentage based on the modelled cohort is reported.

Figures:

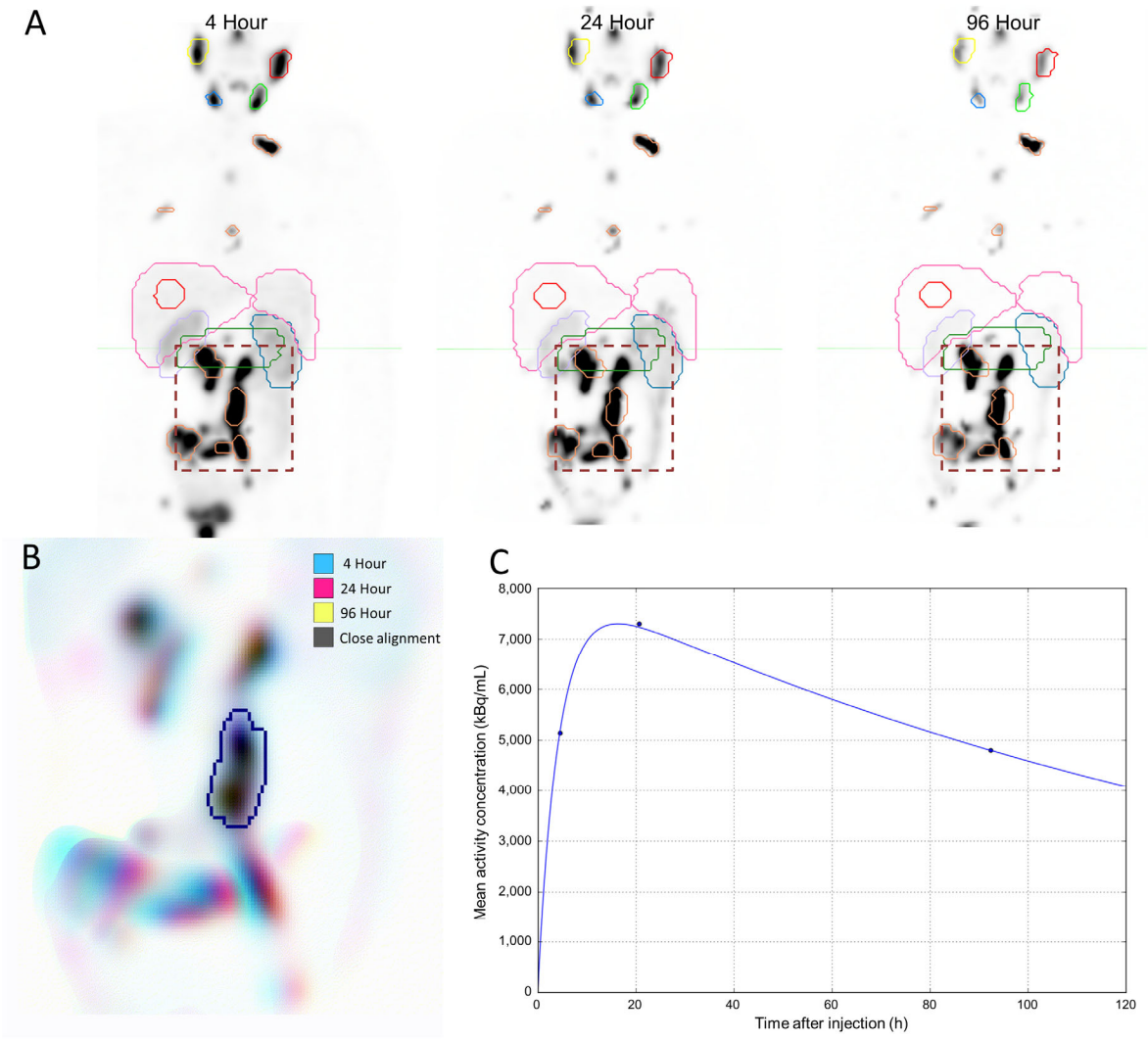

Figure 1 – A) Initial coarse alignment of full image volume for serial 4, 24, & 96h quantitative SPECT images. B) Output of focused image registration based on a contour-defined mask (dashed region of serial MIPs in A). B) Three-color maximum intensity projection is used to verify alignment for serial quantitative SPECT images with 3D contour region highlighted. Black indicates good alignment while color-fringing shows areas with spatial offset C) Three phase exponential curve is generated with exponential parameters taken for population analysis.

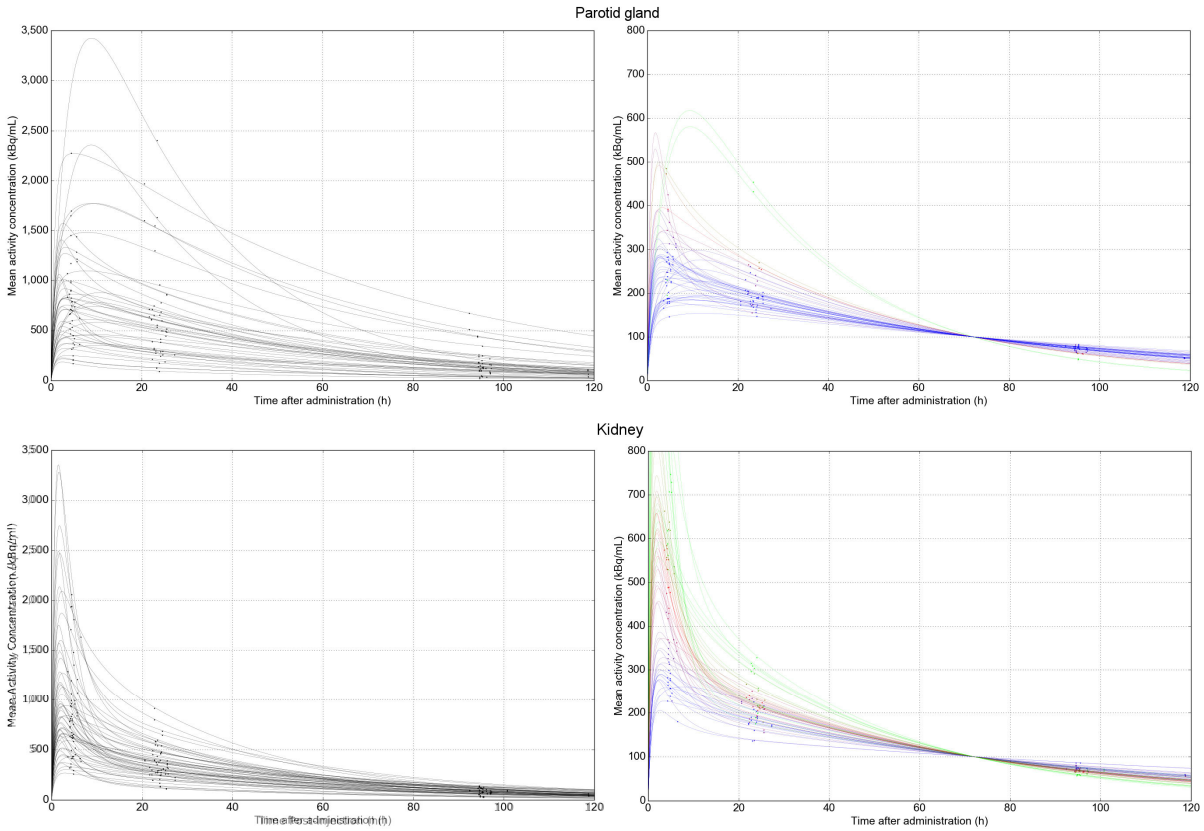

Figure 2 - Population time-activity curves for parotid gland (top-left) and kidney (bottom-left) for ^{177}Lu-PSMA-617 based on serial post-treatment imaging. To calculate time-integrated activity based on single imaging time point, all curves are normalized by amplitude to the single measurement value; in this example 100 kBq/ml at 72 hours post-administration (top & bottom right).

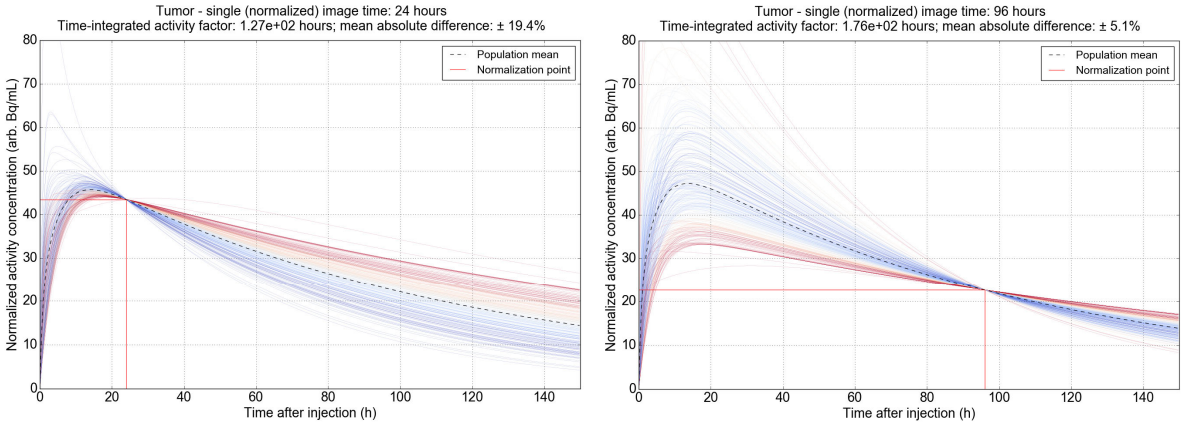

Figure 3 - Population pharmacokinetic models for tumor based on serial imaging of 226 individual lesions. Each chart is normalized to the mean of all curves (dashed line) at 24 (a) and 96 (b) hours. Individual time-activity curves are shaded according to agreement with mean population integral time-integrated activity estimate.

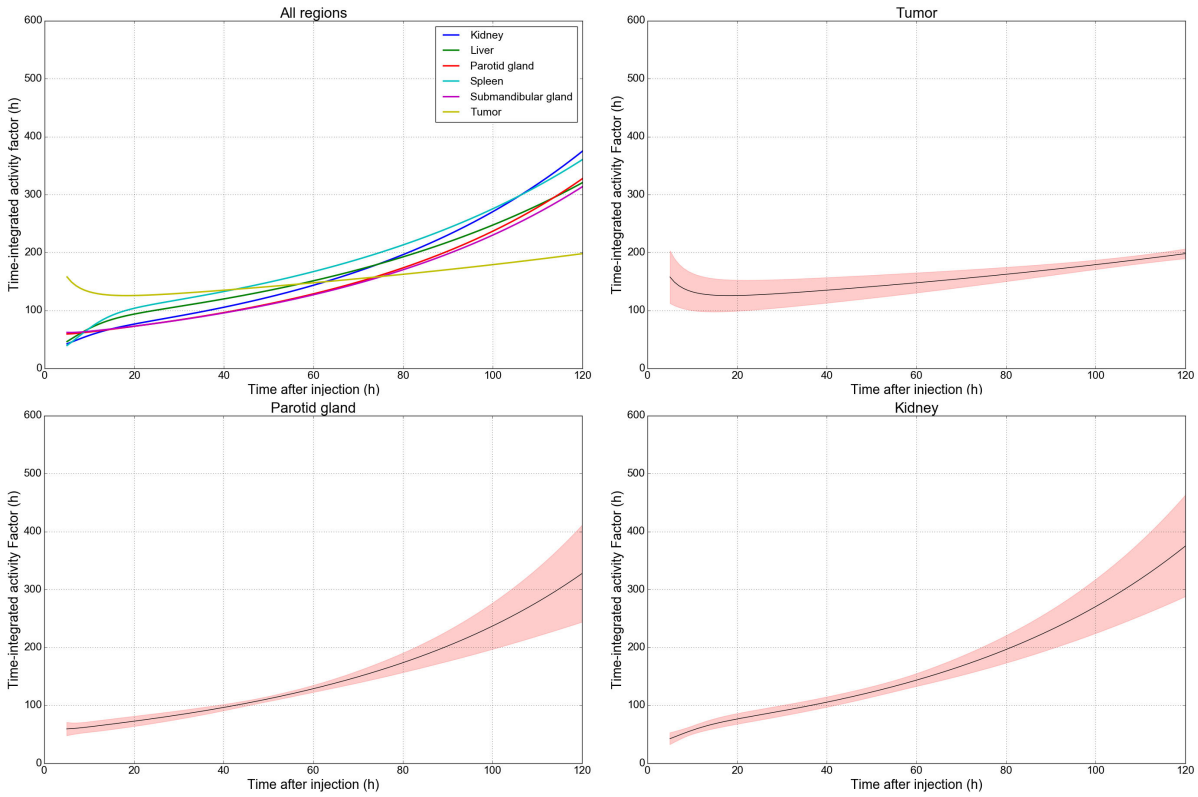

Figure 4 - Single time point factors to translate local tissue activity concentration (Bq/ml) into disintegrations per unit volume (Bq*h/ml) for dosimetry of ^{177}Lu-PSMA-617. Dose factors tumor, parotid glands, and kidneys are shown while all seven considered tissues are illustrated in Supplemental Figure 2. Individual plots include overlay of mean absolute error based on range of modelled time-integrated activity values when normalized to the specified measurement time. Estimates of tumor dosimetry are most accurate using delayed imaging while at-risk tissues benefit from imaging in the first 48 hours post-administration.

Supplementary Data:

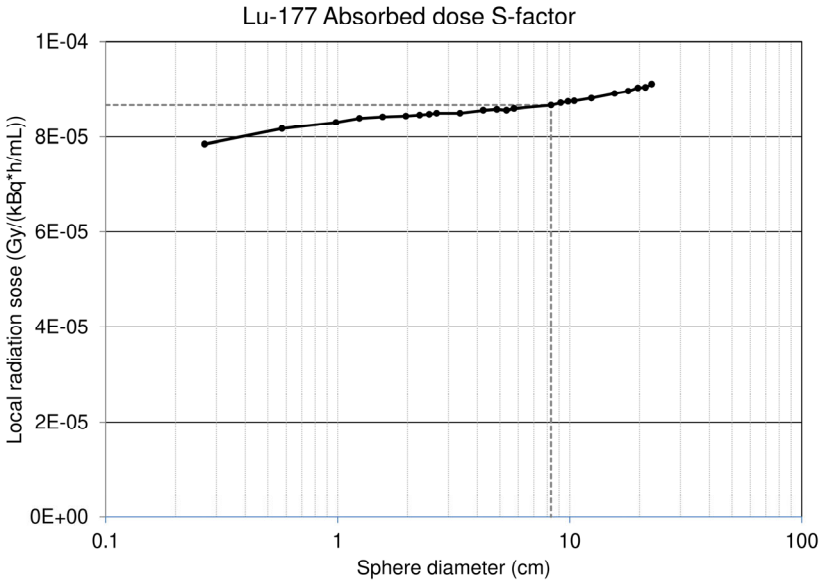

Supplemental Figure 1 - Time-integrated Activity Concentration (kBq*h/ml) to Radiation Absorbed Dose (Gy) S-factors as a function of object diameter for ^{177}Lu according to OLINDA sphere model. For regions with masses between 0.5g and 5,000g the dose factor is within ±5% of 8.67E-5 Gy/(kBq*h/mL)

Image Time (hours)	Submandibular	Tumor	Parotid	Spleen	Kidney	Liver
5	62.1	157.9	59.4	39.6	42.5	46.4
6	62.0	149.0	59.8	45.4	45.5	51.2
7	62.3	142.7	60.5	51.4	48.6	56.0
8	62.7	138.2	61.2	57.6	51.5	60.6
9	63.4	134.7	62.1	63.6	54.4	65.0
10	64.1	132.2	62.9	69.4	57.1	69.1
11	64.8	130.2	63.9	74.8	59.7	72.8
12	65.7	128.8	64.8	79.7	62.1	76.2
13	66.5	127.7	65.8	84.2	64.4	79.2
14	67.4	126.9	66.7	88.1	66.4	82.0
15	68.3	126.4	67.7	91.6	68.4	84.5
16	69.1	126.0	68.7	94.7	70.2	86.7
17	70.1	125.8	69.7	97.4	71.9	88.7
18	71.0	125.7	70.7	99.8	73.5	90.6
19	71.9	125.7	71.7	101.9	75.1	92.3
20	72.9	125.8	72.7	103.8	76.6	93.8
21	73.9	126.0	73.7	105.6	78.0	95.3
22	74.9	126.3	74.8	107.3	79.5	96.8
23	75.9	126.6	75.8	108.8	80.9	98.1
24	76.9	126.9	76.9	110.3	82.2	99.5
25	77.9	127.3	78.0	111.8	83.6	100.8
26	79.0	127.7	79.1	113.2	85.0	102.0
27	80.1	128.1	80.2	114.6	86.4	103.3
28	81.2	128.6	81.4	115.9	87.8	104.5
29	82.3	129.0	82.5	117.3	89.2	105.8
30	83.4	129.5	83.7	118.6	90.6	107.0
31	84.6	130.0	84.9	120.0	92.0	108.3
32	85.7	130.5	86.1	121.4	93.4	109.5
33	86.9	131.1	87.3	122.7	94.9	110.8
34	88.1	131.6	88.6	124.1	96.3	112.1
35	89.3	132.2	89.8	125.5	97.8	113.3
36	90.6	132.7	91.1	126.9	99.3	114.6
37	91.9	133.3	92.4	128.3	100.9	115.9
38	93.1	133.9	93.7	129.8	102.4	117.3
39	94.4	134.4	95.1	131.3	104.0	118.6
40	95.8	135.0	96.4	132.7	105.6	120.0
41	97.1	135.6	97.8	134.2	107.2	121.3
42	98.5	136.2	99.2	135.8	108.9	122.7
43	99.9	136.8	100.7	137.3	110.5	124.2
44	101.3	137.4	102.1	138.9	112.3	125.6
45	102.7	138.1	103.6	140.5	114.0	127.0
46	104.2	138.7	105.1	142.1	115.7	128.5
47	105.7	139.3	106.6	143.7	117.5	130.0
48	107.2	139.9	108.2	145.4	119.3	131.5
49	108.7	140.6	109.7	147.0	121.2	133.0
50	110.3	141.2	111.3	148.7	123.1	134.6
51	111.8	141.9	113.0	150.5	125.0	136.1
52	113.4	142.5	114.6	152.2	126.9	137.7
53	115.1	143.2	116.3	154.0	128.9	139.4
54	116.7	143.8	118.0	155.8	130.9	141.0
55	118.4	144.5	119.7	157.6	132.9	142.7
56	120.1	145.1	121.5	159.5	135.0	144.3
57	121.8	145.8	123.3	161.4	137.1	146.0

58	123.6	146.5	125.1	163.3	139.2	147.8
59	125.4	147.2	126.9	165.2	141.4	149.5
60	127.2	147.9	128.8	167.2	143.6	151.3
61	129.1	148.5	130.7	169.2	145.9	153.1
62	130.9	149.2	132.6	171.2	148.2	154.9
63	132.8	149.9	134.6	173.3	150.5	156.8
64	134.8	150.6	136.6	175.3	152.9	158.7
65	136.7	151.3	138.7	177.5	155.3	160.6
66	138.7	152.1	140.7	179.6	157.7	162.5
67	140.8	152.8	142.8	181.8	160.2	164.5
68	142.8	153.5	145.0	184.0	162.7	166.5
69	144.9	154.2	147.2	186.2	165.3	168.5
70	147.1	154.9	149.4	188.5	167.9	170.5
71	149.2	155.7	151.6	190.8	170.5	172.6
72	151.4	156.4	153.9	193.2	173.2	174.7
73	153.7	157.2	156.2	195.6	176.0	176.8
74	156.0	157.9	158.6	198.0	178.8	179.0
75	158.3	158.7	161.0	200.4	181.6	181.2
76	160.6	159.4	163.5	202.9	184.5	183.4
77	163.0	160.2	165.9	205.5	187.4	185.7
78	165.4	160.9	168.5	208.0	190.4	188.0
79	167.9	161.7	171.1	210.6	193.4	190.3
80	170.4	162.5	173.7	213.3	196.5	192.6
81	172.9	163.3	176.3	216.0	199.7	195.0
82	175.5	164.1	179.1	218.7	202.9	197.4
83	178.2	164.9	181.8	221.5	206.1	199.9
84	180.8	165.7	184.6	224.3	209.4	202.4
85	183.6	166.5	187.5	227.1	212.8	204.9
86	186.3	167.3	190.4	230.0	216.2	207.5
87	189.1	168.1	193.3	233.0	219.7	210.1
88	192.0	168.9	196.4	236.0	223.2	212.7
89	194.9	169.7	199.4	239.0	226.8	215.4
90	197.8	170.5	202.5	242.1	230.4	218.1
91	200.8	171.4	205.7	245.2	234.2	220.9
92	203.9	172.2	208.9	248.4	237.9	223.7
93	207.0	173.1	212.2	251.6	241.8	226.5
94	210.1	173.9	215.6	254.9	245.7	229.4
95	213.3	174.8	219.0	258.2	249.7	232.3
96	216.6	175.6	222.4	261.6	253.7	235.2
97	219.9	176.5	226.0	265.0	257.8	238.2
98	223.3	177.4	229.5	268.5	262.0	241.3
99	226.7	178.3	233.2	272.0	266.3	244.4
100	230.2	179.1	236.9	275.6	270.6	247.5
101	233.7	180.0	240.7	279.2	275.0	250.7
102	237.3	180.9	244.6	283.0	279.5	253.9
103	241.0	181.8	248.5	286.7	284.1	257.2
104	244.7	182.7	252.5	290.5	288.7	260.5
105	248.5	183.7	256.6	294.4	293.5	263.8
106	252.4	184.6	260.7	298.4	298.3	267.3
107	256.3	185.5	265.0	302.4	303.1	270.7
108	260.3	186.4	269.3	306.4	308.1	274.2
109	264.3	187.4	273.7	310.6	313.2	277.8
110	268.4	188.3	278.1	314.7	318.3	281.4
111	272.6	189.3	282.7	319.0	323.6	285.1
112	276.9	190.2	287.3	323.3	328.9	288.8
113	281.2	191.2	292.0	327.7	334.3	292.6

114	285.6	192.2	296.8	332.2	339.9	296.4
115	290.1	193.1	301.7	336.7	345.5	300.3
116	294.7	194.1	306.7	341.4	351.2	304.3
117	299.3	195.1	311.8	346.0	357.0	308.3
118	304.1	196.1	317.0	350.8	362.9	312.4
119	308.9	197.1	322.3	355.6	368.9	316.5
120	313.8	198.1	327.7	360.5	375.1	320.7
121	318.7	199.1	333.2	365.5	381.3	324.9
122	323.8	200.2	338.8	370.6	387.7	329.2
123	328.9	201.2	344.5	375.7	394.1	333.6
124	334.2	202.2	350.3	381.0	400.7	338.1
125	339.5	203.3	356.2	386.3	407.4	342.6
126	344.9	204.3	362.3	391.7	414.2	347.1
127	350.4	205.4	368.4	397.2	421.1	351.8
128	356.0	206.4	374.7	402.8	428.2	356.5
129	361.8	207.5	381.1	408.4	435.3	361.3
130	367.6	208.6	387.7	414.2	442.7	366.1
131	373.5	209.7	394.3	420.1	450.1	371.0
132	379.5	210.8	401.1	426.0	457.7	376.0
133	385.6	211.9	408.1	432.0	465.4	381.1
134	391.8	213.0	415.1	438.2	473.2	386.3
135	398.2	214.1	422.3	444.4	481.2	391.5
136	404.6	215.2	429.7	450.8	489.3	396.8
137	411.2	216.4	437.2	457.2	497.6	402.2
138	417.9	217.5	444.8	463.8	506.0	407.6
139	424.7	218.7	452.7	470.4	514.6	413.2
140	431.6	219.8	460.6	477.2	523.3	418.8
141	438.6	221.0	468.8	484.1	532.2	424.5
142	445.8	222.1	477.0	491.1	541.2	430.3
143	453.1	223.3	485.5	498.2	550.4	436.2
144	460.5	224.5	494.1	505.4	559.8	442.2
145	468.1	225.7	503.0	512.7	569.3	448.2
146	475.8	226.9	512.0	520.2	579.0	454.4
147	483.6	228.1	521.1	527.8	588.9	460.6
148	491.6	229.3	530.5	535.5	598.9	467.0
149	499.7	230.6	540.1	543.3	609.2	473.4

Supplemental Table 1 -Time-integrated activity factors to convert single time point activity concentration (Bq/ml) into estimated decays per unit volume (Bq*h/mL)

Image Time (hours)	Submandibular	Tumor	Parotid	Spleen	Kidney	Liver
5	5.39E-06	1.37E-05	5.15E-06	3.44E-06	3.69E-06	4.03E-06
6	5.38E-06	1.29E-05	5.19E-06	3.94E-06	3.95E-06	4.44E-06
7	5.40E-06	1.24E-05	5.24E-06	4.46E-06	4.21E-06	4.86E-06
8	5.44E-06	1.20E-05	5.31E-06	4.99E-06	4.47E-06	5.26E-06
9	5.49E-06	1.17E-05	5.38E-06	5.52E-06	4.72E-06	5.64E-06
10	5.55E-06	1.15E-05	5.46E-06	6.02E-06	4.95E-06	5.99E-06
11	5.62E-06	1.13E-05	5.54E-06	6.48E-06	5.18E-06	6.31E-06
12	5.69E-06	1.12E-05	5.62E-06	6.91E-06	5.39E-06	6.61E-06
13	5.77E-06	1.11E-05	5.70E-06	7.30E-06	5.58E-06	6.87E-06
14	5.84E-06	1.10E-05	5.78E-06	7.64E-06	5.76E-06	7.11E-06
15	5.92E-06	1.10E-05	5.87E-06	7.94E-06	5.93E-06	7.32E-06
16	6.00E-06	1.09E-05	5.95E-06	8.21E-06	6.09E-06	7.52E-06
17	6.07E-06	1.09E-05	6.04E-06	8.44E-06	6.23E-06	7.69E-06
18	6.16E-06	1.09E-05	6.13E-06	8.65E-06	6.37E-06	7.85E-06
19	6.24E-06	1.09E-05	6.22E-06	8.83E-06	6.51E-06	8.00E-06
20	6.32E-06	1.09E-05	6.30E-06	9.00E-06	6.64E-06	8.14E-06
21	6.40E-06	1.09E-05	6.39E-06	9.16E-06	6.77E-06	8.27E-06
22	6.49E-06	1.09E-05	6.48E-06	9.30E-06	6.89E-06	8.39E-06
23	6.58E-06	1.10E-05	6.58E-06	9.44E-06	7.01E-06	8.51E-06
24	6.67E-06	1.10E-05	6.67E-06	9.57E-06	7.13E-06	8.62E-06
25	6.76E-06	1.10E-05	6.76E-06	9.69E-06	7.25E-06	8.74E-06
26	6.85E-06	1.11E-05	6.86E-06	9.81E-06	7.37E-06	8.85E-06
27	6.94E-06	1.11E-05	6.96E-06	9.93E-06	7.49E-06	8.95E-06
28	7.04E-06	1.11E-05	7.06E-06	1.01E-05	7.61E-06	9.06E-06
29	7.13E-06	1.12E-05	7.16E-06	1.02E-05	7.73E-06	9.17E-06
30	7.23E-06	1.12E-05	7.26E-06	1.03E-05	7.85E-06	9.28E-06
31	7.33E-06	1.13E-05	7.36E-06	1.04E-05	7.97E-06	9.39E-06
32	7.43E-06	1.13E-05	7.46E-06	1.05E-05	8.10E-06	9.50E-06
33	7.54E-06	1.14E-05	7.57E-06	1.06E-05	8.22E-06	9.60E-06
34	7.64E-06	1.14E-05	7.68E-06	1.08E-05	8.35E-06	9.71E-06
35	7.75E-06	1.15E-05	7.79E-06	1.09E-05	8.48E-06	9.83E-06
36	7.85E-06	1.15E-05	7.90E-06	1.10E-05	8.61E-06	9.94E-06
37	7.96E-06	1.16E-05	8.01E-06	1.11E-05	8.74E-06	1.01E-05
38	8.08E-06	1.16E-05	8.13E-06	1.13E-05	8.88E-06	1.02E-05
39	8.19E-06	1.17E-05	8.24E-06	1.14E-05	9.02E-06	1.03E-05
40	8.30E-06	1.17E-05	8.36E-06	1.15E-05	9.15E-06	1.04E-05
41	8.42E-06	1.18E-05	8.48E-06	1.16E-05	9.30E-06	1.05E-05
42	8.54E-06	1.18E-05	8.60E-06	1.18E-05	9.44E-06	1.06E-05
43	8.66E-06	1.19E-05	8.73E-06	1.19E-05	9.58E-06	1.08E-05
44	8.78E-06	1.19E-05	8.85E-06	1.20E-05	9.73E-06	1.09E-05
45	8.91E-06	1.20E-05	8.98E-06	1.22E-05	9.88E-06	1.10E-05
46	9.03E-06	1.20E-05	9.11E-06	1.23E-05	1.00E-05	1.11E-05
47	9.16E-06	1.21E-05	9.24E-06	1.25E-05	1.02E-05	1.13E-05
48	9.29E-06	1.21E-05	9.38E-06	1.26E-05	1.03E-05	1.14E-05
49	9.43E-06	1.22E-05	9.51E-06	1.27E-05	1.05E-05	1.15E-05
50	9.56E-06	1.22E-05	9.65E-06	1.29E-05	1.07E-05	1.17E-05
51	9.70E-06	1.23E-05	9.79E-06	1.30E-05	1.08E-05	1.18E-05

52	9.84E-06	1.24E-05	9.94E-06	1.32E-05	1.10E-05	1.19E-05
53	9.98E-06	1.24E-05	1.01E-05	1.34E-05	1.12E-05	1.21E-05
54	1.01E-05	1.25E-05	1.02E-05	1.35E-05	1.13E-05	1.22E-05
55	1.03E-05	1.25E-05	1.04E-05	1.37E-05	1.15E-05	1.24E-05
56	1.04E-05	1.26E-05	1.05E-05	1.38E-05	1.17E-05	1.25E-05
57	1.06E-05	1.26E-05	1.07E-05	1.40E-05	1.19E-05	1.27E-05
58	1.07E-05	1.27E-05	1.08E-05	1.42E-05	1.21E-05	1.28E-05
59	1.09E-05	1.28E-05	1.10E-05	1.43E-05	1.23E-05	1.30E-05
60	1.10E-05	1.28E-05	1.12E-05	1.45E-05	1.25E-05	1.31E-05
61	1.12E-05	1.29E-05	1.13E-05	1.47E-05	1.26E-05	1.33E-05
62	1.14E-05	1.29E-05	1.15E-05	1.48E-05	1.28E-05	1.34E-05
63	1.15E-05	1.30E-05	1.17E-05	1.50E-05	1.30E-05	1.36E-05
64	1.17E-05	1.31E-05	1.18E-05	1.52E-05	1.33E-05	1.38E-05
65	1.19E-05	1.31E-05	1.20E-05	1.54E-05	1.35E-05	1.39E-05
66	1.20E-05	1.32E-05	1.22E-05	1.56E-05	1.37E-05	1.41E-05
67	1.22E-05	1.32E-05	1.24E-05	1.58E-05	1.39E-05	1.43E-05
68	1.24E-05	1.33E-05	1.26E-05	1.60E-05	1.41E-05	1.44E-05
69	1.26E-05	1.34E-05	1.28E-05	1.61E-05	1.43E-05	1.46E-05
70	1.28E-05	1.34E-05	1.29E-05	1.63E-05	1.46E-05	1.48E-05
71	1.29E-05	1.35E-05	1.31E-05	1.65E-05	1.48E-05	1.50E-05
72	1.31E-05	1.36E-05	1.33E-05	1.67E-05	1.50E-05	1.51E-05
73	1.33E-05	1.36E-05	1.35E-05	1.70E-05	1.53E-05	1.53E-05
74	1.35E-05	1.37E-05	1.38E-05	1.72E-05	1.55E-05	1.55E-05
75	1.37E-05	1.38E-05	1.40E-05	1.74E-05	1.57E-05	1.57E-05
76	1.39E-05	1.38E-05	1.42E-05	1.76E-05	1.60E-05	1.59E-05
77	1.41E-05	1.39E-05	1.44E-05	1.78E-05	1.62E-05	1.61E-05
78	1.43E-05	1.40E-05	1.46E-05	1.80E-05	1.65E-05	1.63E-05
79	1.46E-05	1.40E-05	1.48E-05	1.83E-05	1.68E-05	1.65E-05
80	1.48E-05	1.41E-05	1.51E-05	1.85E-05	1.70E-05	1.67E-05
81	1.50E-05	1.42E-05	1.53E-05	1.87E-05	1.73E-05	1.69E-05
82	1.52E-05	1.42E-05	1.55E-05	1.90E-05	1.76E-05	1.71E-05
83	1.54E-05	1.43E-05	1.58E-05	1.92E-05	1.79E-05	1.73E-05
84	1.57E-05	1.44E-05	1.60E-05	1.94E-05	1.82E-05	1.75E-05
85	1.59E-05	1.44E-05	1.63E-05	1.97E-05	1.84E-05	1.78E-05
86	1.62E-05	1.45E-05	1.65E-05	1.99E-05	1.87E-05	1.80E-05
87	1.64E-05	1.46E-05	1.68E-05	2.02E-05	1.90E-05	1.82E-05
88	1.66E-05	1.46E-05	1.70E-05	2.05E-05	1.94E-05	1.84E-05
89	1.69E-05	1.47E-05	1.73E-05	2.07E-05	1.97E-05	1.87E-05
90	1.72E-05	1.48E-05	1.76E-05	2.10E-05	2.00E-05	1.89E-05
91	1.74E-05	1.49E-05	1.78E-05	2.13E-05	2.03E-05	1.91E-05
92	1.77E-05	1.49E-05	1.81E-05	2.15E-05	2.06E-05	1.94E-05
93	1.79E-05	1.50E-05	1.84E-05	2.18E-05	2.10E-05	1.96E-05
94	1.82E-05	1.51E-05	1.87E-05	2.21E-05	2.13E-05	1.99E-05
95	1.85E-05	1.52E-05	1.90E-05	2.24E-05	2.16E-05	2.01E-05
96	1.88E-05	1.52E-05	1.93E-05	2.27E-05	2.20E-05	2.04E-05
97	1.91E-05	1.53E-05	1.96E-05	2.30E-05	2.24E-05	2.07E-05
98	1.94E-05	1.54E-05	1.99E-05	2.33E-05	2.27E-05	2.09E-05
99	1.97E-05	1.55E-05	2.02E-05	2.36E-05	2.31E-05	2.12E-05
100	2.00E-05	1.55E-05	2.05E-05	2.39E-05	2.35E-05	2.15E-05
101	2.03E-05	1.56E-05	2.09E-05	2.42E-05	2.38E-05	2.17E-05

102	2.06E-05	1.57E-05	2.12E-05	2.45E-05	2.42E-05	2.20E-05
103	2.09E-05	1.58E-05	2.15E-05	2.49E-05	2.46E-05	2.23E-05
104	2.12E-05	1.58E-05	2.19E-05	2.52E-05	2.50E-05	2.26E-05
105	2.15E-05	1.59E-05	2.22E-05	2.55E-05	2.54E-05	2.29E-05
106	2.19E-05	1.60E-05	2.26E-05	2.59E-05	2.59E-05	2.32E-05
107	2.22E-05	1.61E-05	2.30E-05	2.62E-05	2.63E-05	2.35E-05
108	2.26E-05	1.62E-05	2.33E-05	2.66E-05	2.67E-05	2.38E-05
109	2.29E-05	1.62E-05	2.37E-05	2.69E-05	2.72E-05	2.41E-05
110	2.33E-05	1.63E-05	2.41E-05	2.73E-05	2.76E-05	2.44E-05
111	2.36E-05	1.64E-05	2.45E-05	2.77E-05	2.81E-05	2.47E-05
112	2.40E-05	1.65E-05	2.49E-05	2.80E-05	2.85E-05	2.50E-05
113	2.44E-05	1.66E-05	2.53E-05	2.84E-05	2.90E-05	2.54E-05
114	2.48E-05	1.67E-05	2.57E-05	2.88E-05	2.95E-05	2.57E-05
115	2.52E-05	1.67E-05	2.62E-05	2.92E-05	3.00E-05	2.60E-05
116	2.56E-05	1.68E-05	2.66E-05	2.96E-05	3.04E-05	2.64E-05
117	2.60E-05	1.69E-05	2.70E-05	3.00E-05	3.10E-05	2.67E-05
118	2.64E-05	1.70E-05	2.75E-05	3.04E-05	3.15E-05	2.71E-05
119	2.68E-05	1.71E-05	2.79E-05	3.08E-05	3.20E-05	2.74E-05
120	2.72E-05	1.72E-05	2.84E-05	3.13E-05	3.25E-05	2.78E-05
121	2.76E-05	1.73E-05	2.89E-05	3.17E-05	3.31E-05	2.82E-05
122	2.81E-05	1.74E-05	2.94E-05	3.21E-05	3.36E-05	2.85E-05
123	2.85E-05	1.74E-05	2.99E-05	3.26E-05	3.42E-05	2.89E-05
124	2.90E-05	1.75E-05	3.04E-05	3.30E-05	3.47E-05	2.93E-05
125	2.94E-05	1.76E-05	3.09E-05	3.35E-05	3.53E-05	2.97E-05
126	2.99E-05	1.77E-05	3.14E-05	3.40E-05	3.59E-05	3.01E-05
127	3.04E-05	1.78E-05	3.19E-05	3.44E-05	3.65E-05	3.05E-05
128	3.09E-05	1.79E-05	3.25E-05	3.49E-05	3.71E-05	3.09E-05
129	3.14E-05	1.80E-05	3.30E-05	3.54E-05	3.77E-05	3.13E-05
130	3.19E-05	1.81E-05	3.36E-05	3.59E-05	3.84E-05	3.17E-05
131	3.24E-05	1.82E-05	3.42E-05	3.64E-05	3.90E-05	3.22E-05
132	3.29E-05	1.83E-05	3.48E-05	3.69E-05	3.97E-05	3.26E-05
133	3.34E-05	1.84E-05	3.54E-05	3.75E-05	4.03E-05	3.30E-05
134	3.40E-05	1.85E-05	3.60E-05	3.80E-05	4.10E-05	3.35E-05
135	3.45E-05	1.86E-05	3.66E-05	3.85E-05	4.17E-05	3.39E-05
136	3.51E-05	1.87E-05	3.73E-05	3.91E-05	4.24E-05	3.44E-05
137	3.57E-05	1.88E-05	3.79E-05	3.96E-05	4.31E-05	3.49E-05
138	3.62E-05	1.89E-05	3.86E-05	4.02E-05	4.39E-05	3.53E-05
139	3.68E-05	1.90E-05	3.92E-05	4.08E-05	4.46E-05	3.58E-05
140	3.74E-05	1.91E-05	3.99E-05	4.14E-05	4.54E-05	3.63E-05
141	3.80E-05	1.92E-05	4.06E-05	4.20E-05	4.61E-05	3.68E-05
142	3.87E-05	1.93E-05	4.14E-05	4.26E-05	4.69E-05	3.73E-05
143	3.93E-05	1.94E-05	4.21E-05	4.32E-05	4.77E-05	3.78E-05
144	3.99E-05	1.95E-05	4.28E-05	4.38E-05	4.85E-05	3.83E-05
145	4.06E-05	1.96E-05	4.36E-05	4.45E-05	4.94E-05	3.89E-05
146	4.13E-05	1.97E-05	4.44E-05	4.51E-05	5.02E-05	3.94E-05
147	4.19E-05	1.98E-05	4.52E-05	4.58E-05	5.11E-05	3.99E-05
148	4.26E-05	1.99E-05	4.60E-05	4.64E-05	5.19E-05	4.05E-05
149	4.33E-05	2.00E-05	4.68E-05	4.71E-05	5.28E-05	4.10E-05

Supplemental Table 2 - Dose factors to convert single time point measurement of Activity Concentration (Bq/mL) into radiation absorbed dose (Gy) assuming a nominal tissue density of one gram per milliliter (*23*)

Image Time (hours)	Submandibular	Tumor	Parotid	Spleen	Kidney	Liver
5	16.4	25.7	18.2	32.1	22.8	28.5
6	14.9	24.6	16.2	29.7	19.5	27.4
7	14.0	23.9	14.8	27.8	16.9	26.3
8	13.8	23.3	13.8	26.7	14.8	25.5
9	13.7	22.9	13.3	26.1	13.1	25.1
10	13.8	22.6	13.0	25.5	12.4	24.6
11	13.9	22.3	12.8	25.2	12.2	24.1
12	13.9	22.0	12.7	25.0	12.2	23.6
13	13.9	21.7	12.5	24.7	12.2	23.1
14	13.9	21.5	12.3	24.6	12.2	22.9
15	13.8	21.3	12.1	24.5	12.3	22.6
16	13.7	21.1	11.9	24.3	12.3	22.3
17	13.6	20.8	11.6	24.1	12.3	22.0
18	13.5	20.6	11.4	23.8	12.2	21.7
19	13.3	20.4	11.2	23.5	12.1	21.4
20	13.2	20.2	11.0	23.1	11.9	21.0
21	13.0	20.0	10.7	22.7	11.8	20.6
22	12.7	19.8	10.5	22.3	11.6	20.3
23	12.5	19.6	10.2	21.9	11.4	19.9
24	12.3	19.4	10.0	21.4	11.2	19.5
25	12.0	19.2	9.7	21.0	11.0	19.1
26	11.8	18.9	9.4	20.5	10.9	18.7
27	11.5	18.7	9.1	20.0	10.7	18.3
28	11.2	18.5	8.8	19.5	10.5	17.9
29	10.9	18.3	8.6	19.1	10.3	17.5
30	10.6	18.1	8.3	18.6	10.1	17.1
31	10.4	17.9	8.0	18.1	10.0	16.7
32	10.1	17.7	7.7	17.6	9.8	16.3
33	9.8	17.5	7.5	17.1	9.6	16.0
34	9.5	17.3	7.2	16.6	9.4	15.7
35	9.2	17.0	6.9	16.1	9.2	15.3
36	8.9	16.8	6.7	15.6	9.0	15.0
37	8.6	16.6	6.4	15.1	8.9	14.7
38	8.4	16.4	6.1	14.7	8.7	14.3
39	8.1	16.2	5.8	14.3	8.5	14.0
40	7.8	16.0	5.6	14.0	8.4	13.7
41	7.5	15.8	5.3	13.6	8.3	13.4
42	7.3	15.6	5.0	13.3	8.2	13.1
43	7.0	15.4	4.8	13.0	8.1	12.7
44	6.8	15.2	4.5	12.7	7.9	12.4
45	6.6	14.9	4.3	12.4	7.8	12.1
46	6.4	14.7	4.2	12.1	7.7	11.8
47	6.2	14.5	4.0	11.8	7.6	11.5
48	6.0	14.3	3.9	11.6	7.5	11.2
49	5.8	14.1	3.9	11.3	7.4	10.9

50	5.6	13.9	3.9	11.1	7.4	10.6
51	5.4	13.7	3.9	10.9	7.3	10.3
52	5.3	13.5	3.9	10.8	7.3	10.1
53	5.2	13.3	4.0	10.7	7.2	9.8
54	5.1	13.1	4.0	10.6	7.2	9.6
55	5.0	12.8	4.1	10.5	7.2	9.4
56	4.9	12.6	4.2	10.4	7.3	9.2
57	4.9	12.4	4.3	10.3	7.3	9.1
58	4.9	12.2	4.4	10.2	7.4	8.9
59	5.0	12.0	4.5	10.2	7.5	8.7
60	5.0	11.8	4.7	10.2	7.7	8.6
61	5.1	11.6	4.9	10.1	7.8	8.5
62	5.1	11.4	5.1	10.2	8.0	8.4
63	5.2	11.2	5.3	10.2	8.2	8.3
64	5.3	11.0	5.6	10.2	8.5	8.2
65	5.3	10.8	5.8	10.3	8.7	8.2
66	5.4	10.5	6.1	10.4	8.9	8.1
67	5.5	10.3	6.3	10.5	9.1	8.1
68	5.7	10.1	6.6	10.5	9.3	8.1
69	5.8	9.9	6.9	10.7	9.5	8.1
70	6.0	9.7	7.2	10.8	9.7	8.1
71	6.2	9.5	7.5	11.0	10.0	8.1
72	6.4	9.3	7.8	11.2	10.2	8.1
73	6.6	9.1	8.1	11.5	10.4	8.1
74	6.9	8.9	8.4	11.8	10.6	8.1
75	7.1	8.7	8.7	12.0	10.8	8.1
76	7.3	8.5	9.0	12.3	11.1	8.2
77	7.6	8.3	9.4	12.6	11.3	8.2
78	7.8	8.1	9.7	12.8	11.5	8.3
79	8.1	7.9	10.0	13.1	11.7	8.4
80	8.4	7.7	10.3	13.4	12.0	8.5
81	8.6	7.5	10.7	13.6	12.2	8.6
82	8.9	7.3	11.0	13.9	12.4	8.8
83	9.1	7.1	11.4	14.2	12.6	8.9
84	9.4	7.0	11.8	14.5	12.9	9.0
85	9.7	6.8	12.2	14.7	13.1	9.1
86	10.1	6.6	12.5	15.0	13.3	9.3
87	10.4	6.4	12.9	15.3	13.6	9.4
88	10.8	6.3	13.3	15.6	13.8	9.7
89	11.1	6.1	13.7	16.0	14.1	9.9
90	11.5	5.9	14.1	16.3	14.3	10.1
91	11.8	5.8	14.6	16.7	14.5	10.5
92	12.2	5.6	15.0	17.0	14.8	10.8
93	12.5	5.5	15.4	17.4	15.0	11.1
94	12.9	5.3	15.8	17.8	15.3	11.4
95	13.3	5.2	16.3	18.2	15.5	11.7
96	13.6	5.1	16.7	18.6	15.8	12.1
97	14.0	4.9	17.1	19.0	16.1	12.4
98	14.3	4.8	17.6	19.4	16.3	12.7
99	14.7	4.7	18.0	19.8	16.6	13.0

100	15.1	4.6	18.5	20.1	16.8	13.4
101	15.4	4.5	18.9	20.5	17.1	13.7
102	15.8	4.4	19.4	20.9	17.3	14.0
103	16.2	4.4	19.8	21.3	17.6	14.3
104	16.5	4.3	20.3	21.7	17.8	14.6
105	16.9	4.2	20.7	22.1	18.1	15.0
106	17.3	4.2	21.2	22.4	18.4	15.3
107	17.7	4.1	21.6	22.8	18.6	15.6
108	18.0	4.1	22.1	23.2	18.9	15.9
109	18.4	4.0	22.6	23.6	19.2	16.2
110	18.8	4.0	23.0	24.0	19.4	16.6
111	19.2	4.0	23.5	24.3	19.7	16.9
112	19.5	4.0	24.0	24.8	20.0	17.2
113	19.9	4.0	24.5	25.2	20.3	17.5
114	20.3	4.1	24.9	25.6	20.5	17.8
115	20.7	4.1	25.4	26.0	20.8	18.2
116	21.0	4.1	25.9	26.4	21.1	18.5
117	21.4	4.2	26.4	26.9	21.3	18.8
118	21.8	4.3	26.9	27.3	21.6	19.1
119	22.2	4.3	27.4	27.7	21.9	19.4
120	22.6	4.4	27.9	28.1	22.2	19.7
121	22.9	4.5	28.4	28.6	22.4	20.0
122	23.3	4.6	28.9	29.0	22.7	20.4
123	23.7	4.7	29.4	29.4	23.0	20.7
124	24.1	4.8	29.9	29.8	23.3	21.0
125	24.5	4.9	30.4	30.2	23.5	21.3
126	24.9	5.1	30.9	30.7	23.8	21.6
127	25.3	5.2	31.4	31.1	24.1	22.0
128	25.6	5.3	31.9	31.5	24.4	22.3
129	26.0	5.5	32.4	31.9	24.6	22.6
130	26.4	5.6	33.0	32.3	24.9	22.9
131	26.8	5.8	33.5	32.7	25.2	23.3
132	27.2	6.0	34.0	33.2	25.5	23.6
133	27.6	6.2	34.5	33.6	25.8	23.9
134	28.0	6.4	35.1	34.0	26.0	24.2
135	28.4	6.6	35.6	34.4	26.3	24.6
136	28.7	6.8	36.1	34.8	26.6	24.9
137	29.1	7.0	36.7	35.2	26.9	25.2
138	29.5	7.2	37.2	35.6	27.2	25.5
139	29.9	7.4	37.7	36.0	27.5	25.9
140	30.3	7.7	38.3	36.5	27.8	26.2
141	30.7	7.9	38.8	36.9	28.1	26.5
142	31.1	8.1	39.4	37.3	28.4	26.8
143	31.5	8.3	39.9	37.7	28.7	27.1
144	31.9	8.5	40.5	38.1	29.0	27.5
145	32.3	8.8	41.0	38.5	29.3	27.8
146	32.7	9.0	41.6	38.9	29.5	28.1
147	33.1	9.2	42.2	39.3	29.8	28.4
148	33.5	9.4	42.7	39.7	30.1	28.7
149	33.8	9.7	43.3	40.1	30.4	29.0

Supplemental Table 3 - Mean absolute error of population predictions for each organ and time point expressed as a percentage out of 100%

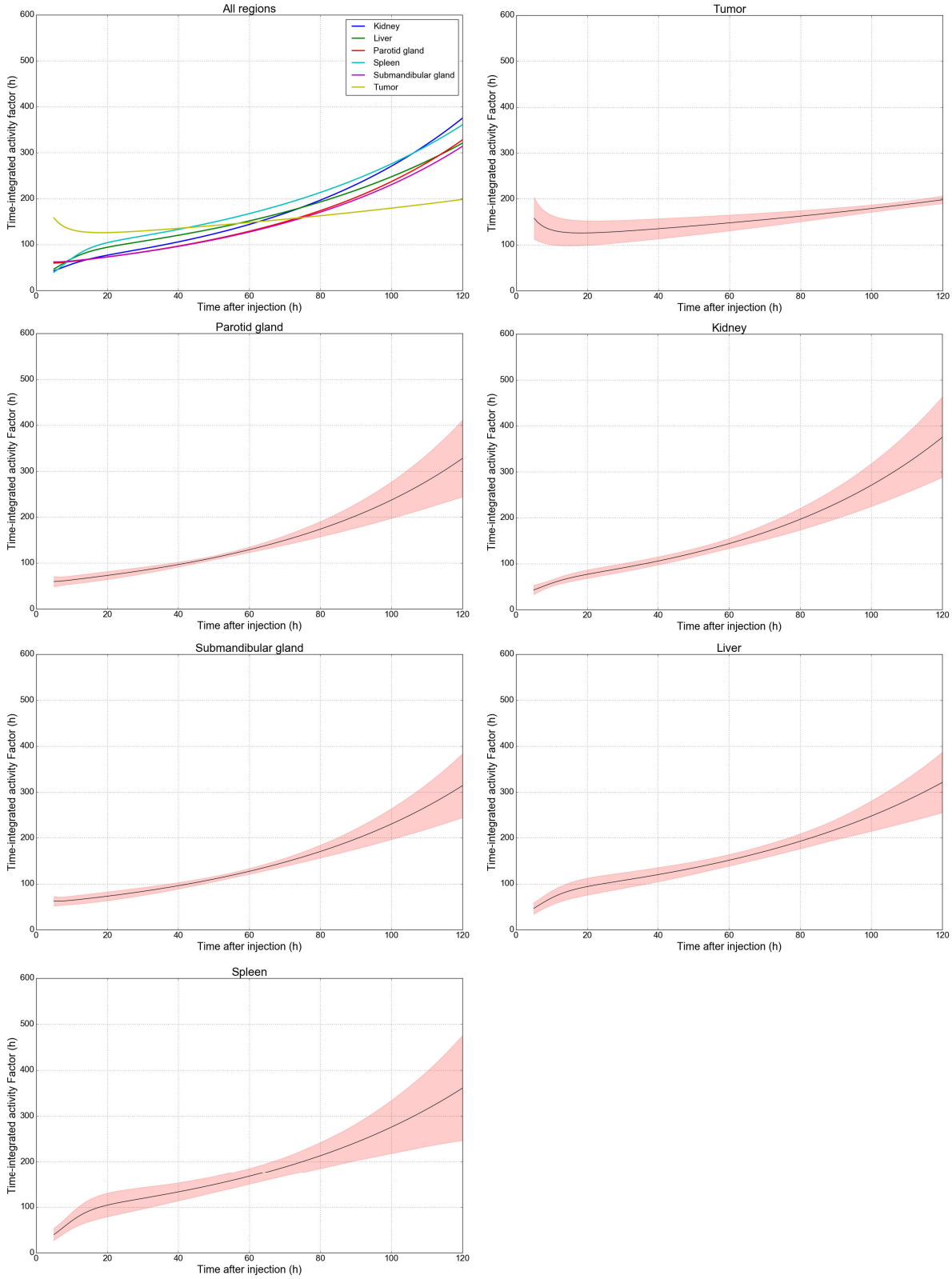
All regions
Kidney
Liver
Parotid gland
Spleen
Submandibular gland
Tumor
Time-integrated activity factor (h)
Time after injection (h)
Tumor
Time-integrated activity Factor (h)
Time after injection (h)
Parotid gland
Time-integrated activity Factor (h)
Time after injection (h)
Kidney
Time-integrated activity Factor (h)
Time after injection (h)
Submandibular gland
Time-integrated activity Factor (h)
Time after injection (h)
Liver
Time-integrated activity Factor (h)
Time after injection (h)
Spleen
Time-integrated activity Factor (h)
Time after injection (h)

Supplemental Figure 2 - Tissue-specific time integrated activity factors for all considered organs. Average deviation from the mean of normalized population values is given in shaded region for each post-treatment image time

$$Activity = -A_1 * e^{-k_1 * t} + A_2 * e^{-k_2 * t} + A_3 * e^{-k_3 * t}$$

$$-A_1 = A_2 + A_3$$

Generic tri-exponential equation used to define organ and tumor time-activity curves. Note negative parameter A_1 denotes uptake phase and the sum of $A_2 + A_3$ equal to $-A_1$ which results in curves that pass through zero at $t=0$ and approaches zero as $t=\infty$.

$$Act(t) = S_p(t) * \left(-A_{p,1} * e^{-k_{p,1} * t} + A_{p,2} * e^{-k_{p,2} * t} + A_{p,3} * e^{-k_{p,3} * t}\right)$$

$$S_p(t) = \frac{Act(t)}{\left(-A_{p,1} * e^{-k_{p,1} * t} + A_{p,2} * e^{-k_{p,2} * t} + A_{p,3} * e^{-k_{p,3} * t}\right)}$$

The time-dependent scaling factor $S_p(t)$ is determined for each time-activity curve to normalize the amplitude to match the single time point measurement $Act(t)$.

$$\tilde{A}_p = \int_0^{\infty} S_p(t) * \left(-A_{p,1} * e^{-k_{p,1} * t} + A_{p,2} * e^{-k_{p,2} * t} + A_{p,3} * e^{-k_{p,3} * t}\right) * dt$$

Time-integrated activity is taken as the area under the curve from $t=0$ to $t=\infty$ for the normalized curve for each region in the population model.

$$\tilde{A}_p = S_p(t) * \left(\frac{-A_{p,1}}{k_{p,1}} + \frac{A_{p,2}}{k_{p,2}} + \frac{A_{p,3}}{k_{p,3}}\right)$$

For equations of exponential decay, the integral may be solved as the ratio of the amplitude parameter, *A*, over the rate parameter, *k*. In this case the time-integral of a single region, $\tilde{A}_p$, is taken as the sum of the three exponential phases is taken and multiplied by the time-dependent scaling factor, $S_p(t)$.

$$\overline{\tilde{A}_p} = \frac{\sum_{p=1}^{n} S_p(t) * \left(\frac{-A_{p,1}}{k_{p,1}} + \frac{A_{p,2}}{k_{p,2}} + \frac{A_{p,3}}{k_{p,3}}\right)}{n}$$

To assess as a population model, the normalized area under each time-activity curve, $\tilde{A}_p$, is assessed for mean across the cohort of *n* cases.